Open Archive Toulouse Archive Ouverte (OATAO)

OATAO is an open access repository that collects the work of Toulouse researchers and makes it freely available over the web where possible

This is an author's version published in: **http://oatao.univ-toulouse.fr/20884**

Official URL: https://doi.org/10.1002/APP.46846

Dynamic relaxations in a bio-based polyamide with enhanced mechanical modulus

G. Haddou,[1,2] A. Roggero,[2] J. Dandurand,[2] E. Dantras ⓘ,[2] P. Ponteins,[1] C. Lacabanne[2]

[1]Assystem Toulouse, 31 300, Toulouse, France
[2]CIRIMAT, Université de Toulouse, Physique des Polymères, 31062, Toulouse Cedex 09, France
Correspondence to: E. Dantras (E-mail: eric.dantras@univ-tlse3.fr)

ABSTRACT: A new grade of bio-based polyamide (PA)—PA *meta*-xylylene diamine 10 (PA mXD 10)—was investigated. Its first interest is that it permits mild processing conditions at about 200 °C. The calorimetric study shows the existence of two cold crystallizations indicative of slow crystallization rate. The glass transition stabilizes at 55 °C. By combining calorimetry with dynamic mechanical analysis and dynamic dielectric spectroscopy, we found a perfect consistency between the set of data giving the molecular mobility. The localized relaxations follow Arrhenius equations while the viscoelastic transition follows a Vogel–Fulcher–Tammann law. The compilation of all the relaxation times determined by means of the different analyses highlights a good correlation. This result is perfectly explained by the polarity of the macromolecular chain. The dynamic mechanical behavior showed a storage modulus higher than for the corresponding aliphatic PA and nearly constant until room temperature. © 2018 Wiley Periodicals, Inc. J. Appl. Polym. Sci. **2018**, *135*, 46846.

INTRODUCTION

Aliphatic polyamides (PAs) are known since decades as engineering polymers due to the presence of hydrogen bonds: the most known are PA 6,6 and PA 6.[1–7] Such polymers are well known for their processability even if they require high temperatures. The main drawback of these PA is the water sensitivity.[8–11] The sorption of water molecules leads to a plasticization of the glass transition and the decrease of mechanical properties. By increasing the length of aliphatic sequences, the water uptake was limited and mild processing conditions are obtained.[12,13] PA 11 and PA 12 were developed along those lines.[14–17]

In parallel, the development of aromatic PAs is sustained by very attractive applications as thermostable polymers.[18–22] For a better processing in industrial conditions, semi-aromatic PAs were designed.[18,23,24]

In the last decade, a lot of research was devoted to bio-based PAs.[25–29] The strategy is to enhance the mechanical properties of classical bio-based PAs like PA 11. Following this line, Arkema proposed the PA *meta*-xylylene diamine 10 (PA mXD 10).[30] This PA is constituted by an alternation of a phenyl ring and an aliphatic sequence in order to reach technical mechanical properties and mild processing temperature. In a first part of this study, the thermal behavior of PA mXD 10 is investigated by differential scanning calorimetry. Then, the investigations

focus mainly on the molecular mobility of PA mXD 10 under mechanical and dielectric solicitations. The influence of hydration on the relaxation modes is shown. The combination of calorimetric, mechanical, and dielectric analyses will allow us to determine the molecular origin of the dynamic behavior of PA mXD 10.

EXPERIMENTAL

Materials
PA mXD 10 is a semicrystalline thermoplastic supplied by Arkema (France). Its structure is illustrated in Figure 1.

As received pellets of PA mXD 10 were hot pressed at 210 °C, 10 MPa for 15 min. Two aluminum plates were used to obtain a homogeneous thickness of the film thanks to the flexibility of the polymeric chain. The dimensions of the samples depend on the test to perform as follows:

- for calorimetric tests, the samples (about 12 mg) were extracted from a film of PA mXD 10,
- for mechanical tests, rectangular parallelepipeds about 50 mm × 10 mm × 0.65 mm were directly processed into a mold with good dimensions,
- for dielectric analyses, disks with a diameter about 40 mm and a thickness around 0.1 mm were extracted from the same disk than the calorimetric samples.
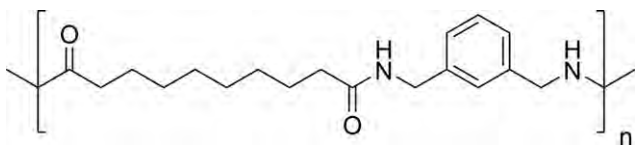
Figure 1. Structure of the PA mXD 10.

Differential scanning calorimetry (DSC), dynamic mechanical thermal analyses (DMA), and dynamic dielectric spectroscopy (DDS) data presented in the manuscript are the compilation of results recorded on six different samples. During the first heating, the water content of PA mXD 10, as determined from water sorption experiments, was 1.3% ± 0.2%. During the second consecutive heating, it is 0% due to evaporation.

Methods

Differential Scanning Calorimetry. DSC was performed on a Diamond DSC (Perkin Elmer, Massachusetts, USA). The samples were placed in closed aluminum pans. They were characterized, under helium atmosphere allowing to reach the lower temperature, in the range 0–250 °C, at 10 °C min^{-1}, in order to erase the thermal history of the polymer. Then, they were cooled from 250 to 0 °C at 10 °C min^{-1}, in order to crystallize the polymer. Finally, the samples were heated a second time, immediately after cooling, to determine the influence of the water evaporation.

Dynamic Mechanical Thermal Analysis. DMA were performed using an Advanced Rheometric Expansion System set up (Rheometric Scientific, USA). The measurements were performed in the rectangular torsional mode, from −140 to 150 °C, with a heating rate of 3 °C min^{-1}, under nitrogen flow, at a frequency of 1 rad s^{-1}, with a dynamic shear strain of 0.1%. The complex shear modulus G* is defined by eq. (1)

$$G^*(\omega, T) = G'(\omega, T) + iG''(\omega, T) \tag{1}$$

where G' is the storage modulus and G'' is the loss modulus.

Dynamic Dielectric Spectroscopy. DDS was made on an impedance analyzer BDS 4000 (Novocontrol technologies GmbH & Co., Germany). The samples were placed between gold-plated stainless steel electrodes (Ø = 40 mm). The measures were performed isothermally from −150 to 150 °C, with a step of 5 °C, in a frequency range from 10^{-2} Hz to 10^6 Hz. The complex permittivity ε* is calculated from the measurement of the complex impedance Z* according to eq. (2)

$$\varepsilon^*(\omega, T) = \varepsilon'(\omega, T) - i\varepsilon''(\omega, T) = \frac{1}{i\omega C_0 Z^*(\omega, T)} \tag{2}$$

where ε' and ε'' are, respectively, the real component and the imaginary component of the dielectric permittivity.

RESULTS AND DISCUSSION

Calorimetric Behavior

Consecutive scans of PA mXD 10 are represented in Figure 2. In the first scan, the curve reveals four events: a step at 35 °C related to the glass transition temperature T_g with a superimposed endothermic peak which is the manifestation of the physical ageing; two exothermic peaks T_{c1} and T_{c2}, at 78 °C and 106 °C,
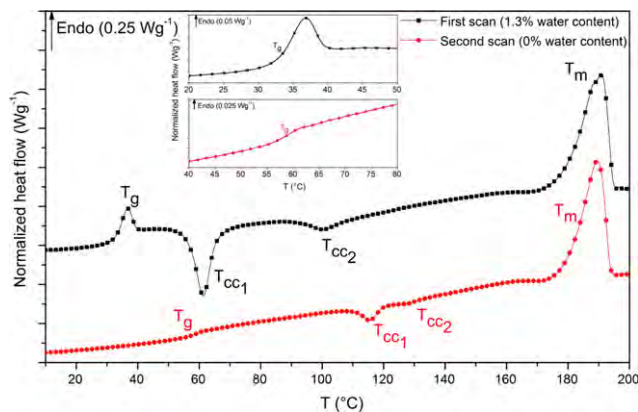

Figure 2. DSC curves of PA mXD 10. A zoom-in of the glass transitions for each heating id reported in the insert. [Color figure can be viewed at wileyonlinelibrary.com]

associated with cold crystallizations of crystallites with different morphologies; and only one wide melting point T_m at 189 °C. The different crystallites melt at close temperature. For the second scan, the glass transition is shifted to 58 °C. Since the thermal history was erased, there is no physical ageing superimposed onto the T_g step. The polymer absorbed water molecules due to the presence of hydrophilic amide groups. It is well known that water plasticized the PAs.[2,4,9–11] At room humidity, the water uptake is 1.3% ± 0.2% wt that is enough to influence the molecular mobility of the amorphous phase. Moreover, the cold crystallizations are shifted toward higher temperatures. This shift can be attributed to the drying of the sample. The significant decrease of the magnitude of the cold crystallization peak indicates that the sample is not fully crystallized due to a cooling faster than the crystallization kinetic of PA mXD 10. This effect on the crystallization kinetic may be attributed to the presence of the aromatic ring on the main chains. The melting temperature is unmodified but the melting peak is thinner and an exothermic event occurs before the peak. This phenomenon is related to the melting/reorganization/recrystallization phenomenon.[12,31,32] All the data are indexed in Table I. The crystalline ratio was determined according to eq. (3).

$$\chi(\%) = \frac{\Delta H_m - \sum \Delta H_{cc}}{\Delta H_\infty} \tag{3}$$

where χ is the crystallinity ratio, ΔH_m is the measured melting enthalpy, $\sum \Delta H_{cc}$ is the sum of measured enthalpies of the cold crystallizations, and ΔH_∞ is the theoretical melting enthalpy of 100% crystallized polymer. The value used here is 244 J g^{-1} which is the enthalpy of 100% crystallized PA 11.[33] This value was chosen due to the close structures between PA 11 and PA mXD 10. Moreover, this is a comparative investigation, not a quantitative one, so the error is negligible. In this study, the crystallinity was calculated about 9% for the first scan and 12% for the second. This difference is due to a cooling after processing faster than the one employed here (10 °C min^{-1}).

The T_g/T_m ratio was calculated and is about 0.7. This result is consistent with the van Krevelen relation valid for a majority of unsymmetrical polymers.[34]

Table I. Thermal Characteristics of PA mXD 10[a]

Scan	T_g (°C)	T_{cc1} (°C)	ΔH_{cc1} (J g^{-1})	T_{cc2} (°C)	ΔH_{cc2} (J g^{-1})	T_m (°C)	ΔH_m (J g^{-1})	χ (%)	T_g/T_m ratio
1st	37 (3)	62 (2)	−17.52 (0.03)	122 (5)	−7.77 (0.08)	188 (2)	48.08(0.03)	9.34 (0.05)	0.672 (0.009)
2nd	55 (2)	111 (1)	−8.23 (0.01)	127 (3)	−4.6 (0.1)	189 (2)	42.11 (0.02)	12.00 (0.05)	0.710 (0.007)

[a] Standard deviations are between brackets.

Mechanical Behavior

Figure 3 shows the different components of the complex shear modulus $G^*(\omega)$ recorded at 1 Hz, as a function of temperature: The storage modulus G', in filled symbols, and the loss modulus G'', open symbols. At 1.3% water content, at low temperature, there is a feeble step at −83 °C on the storage modulus. This step is the β_2 relaxation, associated with the amide–water interactions. At 39 °C, there is a sharp step. This relaxation, called α relaxation, is related to the mechanical manifestation of the glass transition, which is consistent with the calorimetric results. These relaxations are typical of the polymers from PA family.[2,9,35,36] Beyond the α relaxation, the storage modulus increases. Occurring at 72 °C, this improvement is the expression of the cold crystallization.

After drying, the relaxations are significantly modified. The α relaxation is shifted toward 60 °C. As observed by DSC, this improvement can be explained by the water desorption during the first scan. The β_2 relaxation disappears and another weak and wide relaxation appears at −58 °C. This component noted β_1,[9,37] is usually highlighted for the dried specimens of PA and is associated with the amide–amide interactions. The β_1 relaxation is hidden by the β_2 mode, in the presence of water molecules.

The temperature dependence of the dynamic mechanical modulus of PA mXD 10 is analogous with the one of PA 11. For both polymers, the viscoelastic region occurs around 50 °C so that both are glassy below this temperature and rubbery above this temperature. For the glassy state, the storage modulus (glassy modulus) has been measured at 0 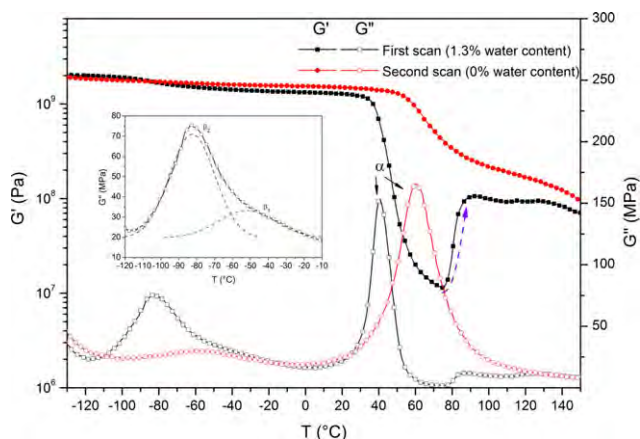°C: it is about 1.32 GPa for PA mXD 10, instead of 0.53 GPa for PA 11. For the rubbery state, the storage modulus (rubbery modulus) has been recorded at 100 °C, it is 0.22 GPa for PA mXD 10 instead of 0.09 GPa for PA 11.[38] It is important to note that the storage modulus is higher for PA mXD 10 than for PA11 in the whole temperature range. This increase is a classical consequence of the introduction of the phenylene groups on the PA chain. The challenge was to optimize the conservative modulus without any increase of transition temperatures.

Dielectric Behavior

The dielectric loss after Kramers–Kronig transform is represented in Figure 4, for the samples at 1.3% water content. The Kramers–Kronig transform allows us to suppress the ohmic conduction which can hide the dielectric relaxations. In Figure 4, three events are observed in addition to the relaxations previously observed in DMA. At the lowest temperature, the γ relaxation is observed: this relaxation is associated with the mobility of the ethylene sequences between two polar groups.[2,35] Above the α relaxation, the Maxwell–Wagner–Sillars (MWS) phenomenon is related to heterogeneities induced by crystalline/amorphous interfaces.[39] At highest temperature and lowest frequency, the dielectric loss greatly increases due to the conduction front labeled σ.

For a better understanding of the relaxation evolution, the mean relaxation times were determined thanks to the Havriliak–Negami equation, defined by eq. (4)

Figure 3. First and second DMA scans of PA mXD 10 at 1 rad s^{-1}. The filled symbols represent the storage modulus G' and the empty symbols the loss modulus G''. A zoom-in of the β_1 and β_2 relaxations is reported in the insert. [Color figure can be viewed at wileyonlinelibrary.com]
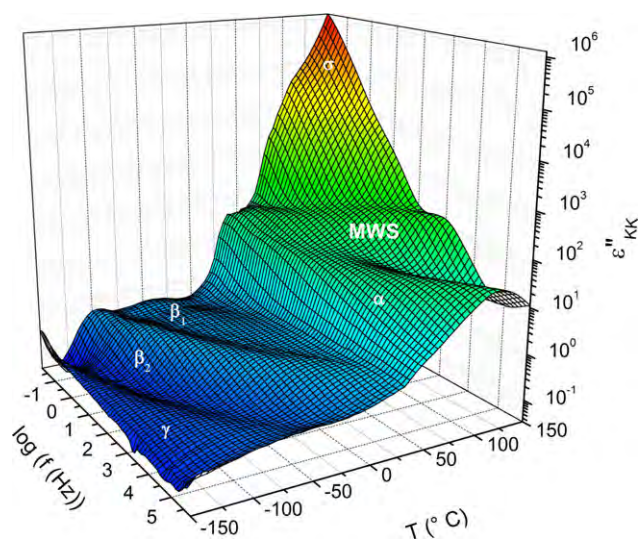

Figure 4. 3D spectrum of dielectric loss versus frequency and temperature after Kramers–Kronig transform at 1.3% water content. [Color figure can be viewed at wileyonlinelibrary.com]
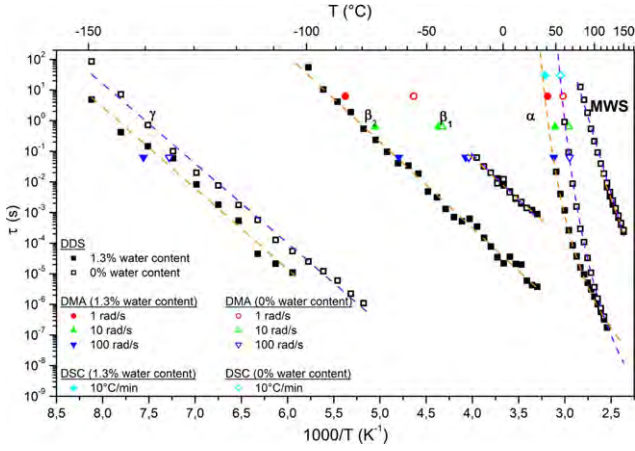
Figure 5. Arrhenius plot of relaxation times of PA mXD 10 at 0% and 1.3% water content. (the dashed lines represent the Arrhenius and VFT fits). [Color figure can be viewed at wileyonlinelibrary.com]

$$\varepsilon^* = \varepsilon_\infty + \frac{\varepsilon_S - \varepsilon_\infty}{\left(1 + (i\omega\tau_{HN})^{\alpha_{HN}}\right)^{\beta_{HN}}} \qquad (4)$$

where ε_∞ is the high-frequency limit of the relative real permittivity, ε_S is the low-frequency limit of the relative real permittivity, ω is the angular frequency and α_{HN} and β_{HN} are the Havriliak–Negami fit parameters, respectively related to the width and the symmetry of the distribution.

All the relaxation times are plotted on the Arrhenius diagram in Figure 5. The localized modes γ, β_1, and β_2 have an Arrhenius behavior described by eq. (5)

$$\tau(T) = \tau_{0a} e^{\frac{E_a}{RT}} \qquad (5)$$

where τ_{0a} is the pre-exponential factor, ΔH is the activation enthalpy, R is the gas constant.

The α relaxation follows the Vogel–Fulcher–Tammann (VFT) behavior described by eq. (6).

$$\tau(T) = \tau_{0v} e^{\frac{1}{\alpha_f (T - T_\infty)}} \qquad (6)$$

where τ_{0v} is the pre-exponential factor, α_f is the free volume thermal expansion coefficient, and T_∞ is the Vogel temperature.

Table II. Parameters of the Arrhenius Fits[a] of the γ, β_1, β_2 Relaxations and MWS Phenomenon

Dielectric phenomena	1.3% water content		0% water content	
	E_a (kJ mol^{-1})	τ_{0a} (s)	E_a (kJ mol^{-1})	τ_{0a} (s)
γ	50 (1)	1.9×10^{-21}	49 (2)	5.5×10^{-20}
β_2	54 (1)	1.1×10^{-15}	—	—
β_1	53 (3)	1.0×10^{-13}	54 (5)	6.7×10^{-15}
MWS	151 (2)	4.8×10^{-23}	191 (4)	4.7×10^{-28}

[a] Standard deviations are between brackets.

Table III. VFT Parameters of α Relaxation[a]

Mode	Water content	T_∞ (°C)	α_f (10^{-4} K^{-1})	τ_{0v} (s)	D
α	1.3%	−3 (5)	9 (1)	5.2×10^{-11}	4.1 (0.5)
	0%	7 (3)	6 (1)	2.3×10^{-13}	6.0 (0.5)

[a] Standard deviations are indicated between brackets.

The parameters from Arrhenius behavior for sub-glassy relaxations are reported in Table II.

Various frequencies were investigated in DMA in addition to the previous tests: 10 rad s^{-1} and 100 rad s^{-1}. In the case of 100 rad s^{-1}, the shift toward higher temperature of the relaxations allows us to observe the γ mode. In Figure 5, the mechanical relaxation times were reported. The DMA results are consistent with the law fits, except for the γ mode that exhibits a lower relaxation time. These discrepancies can be explained by the solicited groups: DMA transmitted the shear loads, independent from dipole groups while DDS solicitation is function of dipoles in the polymer.[40–42] Moreover, the γ relaxation shifts to higher temperatures after drying. This can be explained by the water evaporation that modified the ethylene sequences environment.

As the sub-glassy relaxations have the same behaviors than the usual PA, we will focus on the α relaxation, as displayed on Figure 6. The parameters from VFT fits are reported in Table III. After drying, the Vogel temperature T_∞ increases while the thermal expansion coefficient of the free volume α_f decreases.

An intersection of the fit curves can be observed about 116 °C. The fragility index, noted as D, was calculated, according to Angell.[43,44] It is about 4 at 1.3% water content and 6 after drying. This is the same order of magnitude than the PA 11.[45]

Dynamic Behavior

A compilation of DSC, DMA, and DDS data has been performed in order to describe the dynamic behavior of PA mXD 10 in a broad temperature and frequency range. For DSC results, an equivalent frequency f_{eq}^{DSC} was estimated according to eq. (7).[46,47]
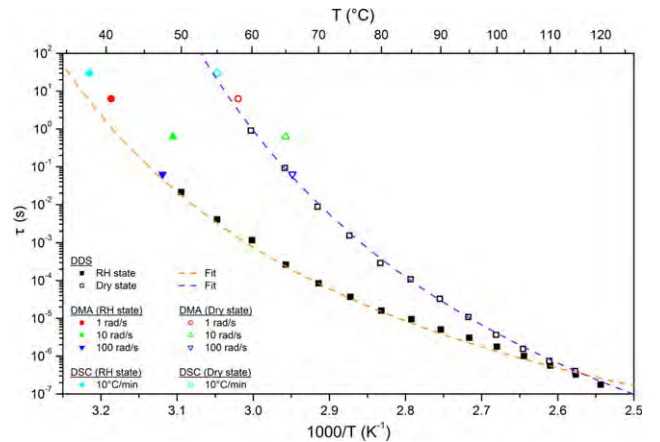

Figure 6. Arrhenius diagram of the α relaxation times and VFT fits (the dashed lines represent the VFT fits). [Color figure can be viewed at wileyonlinelibrary.com]

$$f_{eq}^{DSC} \approx \frac{q}{2\pi a \delta T} \qquad (7)$$

where q is the heating rate, a is a constant nearly equal to 1, and δT is the extent of the glass transition.

The equivalent frequency was found around 5.3×10^{-2} Hz. An associated relaxation time τ_{eq}^{DSC} was calculated from eq. (8)

$$\tau_{eq}^{DSC} = \frac{1}{2\pi f_{eq}^{DSC}} \qquad (8)$$

The obtained value is 30 s. This result is consistent with the VFT fit previously determined.

As shown in Figure 6, the results obtained by DSC and DMA are close to the VFT fit determined from the DDS data. Due to the polarity of the polymeric chain, DMA and DDS involve the same molecular entities of PA mXD 10. Moreover, around the glass transition, the chain sequences implied in the α relaxation as shown by DMA and DDS are also involved in the DSC step. An excellent correlation between the different methods is highlighted through the Arrhenius diagram. A precise representation of the molecular mobility at different scales involved in this polymer is proposed. The compilation of these data provides the set of parameters necessary for making prediction of the dynamic mechanical behavior of PA mXD 10 as a function of temperature and frequency.

CONCLUSIONS

A new grade of bio-based PA—PA mXD 10—was investigated. After saturation at room humidity, the calorimetric study showed a glass transition temperature at 35 °C, two cold crystallizations, and a melting peak at 189 °C. After temperature scans, the T_g was stabilized at 55 °C, while the melting peak was unmodified. The T_g shift may be explained by the presence, in the initial state, of water that plasticizes the polymer.

By DMA, the mechanical behavior of PA mXD 10 exhibits a storage modulus higher than for PA with analogous aliphatic sequence, such as PA 11. In addition, the value of the storage modulus was nearly constant until room temperature. The α relaxation, related to the mechanical manifestation of the viscoelastic transition, was subjected to the same shift than the glass transition measured by DSC. The localized relaxations β_1 and β_2, respectively, associated with the amide–amide interactions and amide–water interactions exhibited behaviors close to usual PA.

Using DDS, in the low temperature range, the γ relaxation, related to the mobility of ethylene sequences, and also β_1 and β_2 relaxations showed Arrhenius behaviors. The α relaxation followed a VFT behavior. The influence of water molecules is also observed on the α relaxation: the Vogel temperature T_∞ increased, after drying. All the relaxation times were displayed on an Arrhenius diagram, including the ones determined from DSC and DMA results: this representation allowed us to highlight an excellent correlation between all the methods.

Finally, this study demonstrated that PA mXD 10 fulfills the requirement of mild processing conditions and restricted water uptake. Its specific interest regarding aliphatic PAs like PA 11 is

the value of its storage modulus: 1.32 GPa. The compilation of thermal, dielectric, and mechanical data allows us to predict the dynamic behavior in a broad frequency and temperature range.

REFERENCES

1. Turi, E. Thermal Characterization of Polymeric Materials; Academic Press: San Diego, **1997**.

2. Prevorsek, D. C.; Butler, R. H.; Reimschuessel, H. K. J. Polym. Sci. Part A-2: Polym. Phys. **1971**, 9, 867.

3. Holmes, D. R.; Bunn, C. W.; Smith, D. J. J. Polym. Sci. **1955**, 17, 159.

4. Xenopoulos, A.; Wunderlich, B. J. Polym. Sci. Part B: Polym. Phys. **1990**, 28, 2271.

5. Greco, R.; Nicolais, L. Polymer (Guildf) **1976**, 17, 1049.

6. Xenopoulos, A.; Wunderlich, B. Polymer (Guildf) **1990**, 31, 1260.

7. Füllbrandt, M.; Wellert, S.; Von Klitzing, R.; Schönhals, A. Polymer **2015**, 75, 34.

8. Lim, L.; Britt, I. J.; Tung, M. A. J. Appl. Polym. Sci. **1999**, 71, 197.

9. Kolařík, J.; Janáček, J. J. Polym. Sci. Part C: Polym. Symp. **2007**, 16, 441.

10. Laredo, E.; Hernandez, M. C. J. Polym. Sci. Part B: Polym. Phys. **1997**, 35, 2879.

11. Laredo, E.; Grimau, M.; Sanchez, F.; Bello, A. Macromolecules **2003**, 36, 9840.

12. Menczel, J. D.; Judovits, L.; Prime, R. B.; Bair, H. E.; Reading, M.; Swier, S. Thermal Analysis of Polymers: Fundamentals and Applications; Wiley: Hoboken, New Jersey, **2009**.

13. Li, Y.; Zhu, X.; Tian, G.; Yan, D.; Zhou, E. Polym. Int. **2001**, 50, 677.

14. Gogolewski, S. Colloid Polym. Sci. **1979**, 257, 811.

15. Ibos, L.; Maraval, C.; Bernès, A.; Teyssèdre, G.; Lacabanne, C.; Wu, S.-L.; Scheinbeim, J. I. J. Polym. Sci. Part B: Polym. Phys. **1999**, 37, 715.

16. Neagu, R. M.; Neagu, E.; Kyritsis, A.; Pissis, P. J. Phys. D: Appl. Phys. **2000**, 33, 1921.

17. Okamba-Diogo, O.; Richaud, E.; Verdu, J.; Fernagut, F.; Guilment, J.; Fayolle, B. Polym. Degrad. Stab. **2015**, 120, 76.

18. Rao, Y.; Waddon, A. J.; Farris, R. J. Polymer (Guildf) **2001**, 42, 5925.

19. Lee, Y. S.; Wetzel, E. D.; Wagner, N. J. J. Mater. Sci. **2003**, 38, 2825.

20. Cheeseman, B. A.; Bogetti, T. A. Compos. Struct. **2003**, 61, 161.

21. Foo, C. C.; Chai, G. B.; Seah, L. K. *Compos. Struct.* **2007**, *80*, 588.

22. Aktay, L.; Johnson, A. F.; Holzapfel, M. *Comput. Mater. Sci.* **2005**, *32*, 252.

23. Papaspyrides, C. D.; Porfyris, A. D.; Rulkens, R.; Grolman, E.; Kolkman, A. J. *J. Polym. Sci. Part A: Polym. Chem.* **2016**, *54*, 2493.

24. Beaume, F.; Laupretre, F.; Monnerie, L.; Maxwell, A.; Davies, G. R. *Polymer (Guildf)* **2000**, *41*, 2677.

25. Cureton, L. T.; Napadensky, E.; Annunziato, C.; La Scala, J. J. *J. Appl. Polym. Sci.* **2017**, 134, DOI: 10.1002/app.45514.

26. Jin, X.; Sun, J.; Zhang, J. S.; Gu, X.; Bourbigot, S.; Li, H.; Tang, W.; Zhang, S. *ACS Appl. Mater. Interfaces* **2017**, *9*, 24964.

27. Wang, S.; Wu, X.; Zhang, X.; Niu, H.; Wang, C.; Zhang, Y.; Bai, X.; Wang, W.; Hou, Y. *Eur. Polym. J.* **2017**, *93*, 368.

28. Wróblewska, A. A.; Bernaerts, K. V.; De Wildeman, S. M. A. *Polymer (Guildf)* **2017**, *124*, 252.

29. Winnacker, M.; Rieger, B. *Macromol. Rapid Commun.* **2016**, *37*, 1391.

30. Arkema, B. Brule, P. Bussi, N. Devaux, M. WO 2010/015772 A1 (**2010**).

31. Wunderlich, B. *Kolloid-Zeitschrift Zeitschrift Für Polym.* **1969**, *231*, 605.

32. Chabert, B.; Chauchard, J.; Cinquin, J. *Makromol. Chem. Macromol. Symp.* **1987**, *9*, 99.

33. Wunderlich, B. Thermal Analysis of Polymeric Materials; Springer-Verlag: Berlin/Heidelberg, **2005**.

34. VanKrevelen, D. W. Properties of Polymers, 2nd ed.; Elsevier, Amsterdam, **1976**.

35. McCrum, N. G.; Read, B. E.; Williams, G. An Elastic and Dielectric Effects in Polymeric Solids; Wiley: New-York, **1967**.

36. Capsal, J. F.; Pousserot, C.; Dantras, E.; Dandurand, J.; Lacabanne, C. *Polymer (Guildf)* **2010**, *51*, 5207.

37. Frank, B.; Frübing, P.; Pissis, P. *J. Polym. Sci. Part B: Polym. Phys.* **1996**, *34*, 1853.

38. Carponcin, D. PhD thesis Université De Toulouse III—Paul Sabatier, **2012**.

39. Smyth, C. P. Dielectric Behavior and Structure; McGraw-Hill book Company, New York, **1955**.

40. Bareš, J. *Collect. Czechoslov. Chem. Commun.* **1967**, *32*, 2640.

41. Janáček, J. *J. Macromol. Sci. Part C: Polym. Rev.* **1973**, 9, 3.

42. Hartwig, G. Dielectric Properties and Their Correlations. In: Polymer Properties at Room and Cryogenic Temperatures. The International Cryogenics Monograph Series. Springer, Boston, MA.

43. Angell, C. A. *J. Non-Cryst. Solids* **1991**, *131–133*, 13.

44. Bressel, R. D.; Angell, C. A. *J. Phys. Chem.* **1972**, *1086*, 3244.

45. Capsal, J.-F. PhD thesis Université De Toulouse III—Paul Sabatier, **2008**.

46. Hensel, A.; Dobbertin, J.; Schawe, J. E. K.; Boller, A.; Schick, C. *J. Therm. Anal.* **1996**, *46*, 935.

47. Donth, E.-J. Relaxation and Thermodynamics in Polymers: Glass Transition; Akademie Verlag: Berlin, **1994**.